Journal Pre-proof

Platinum(II) ring-fused chlorins as efficient theranostic agents: Dyes for tumor-imaging and photodynamic therapy of cancer

Mafalda Laranjo, Márcia Campos Aguiar, Nelson A.M. Pereira, Gonçalo Brites, Bruno F.O. Nascimento, Ana Brito, João Casalta-Lopes, Ana Cristina Gonçalves, Ana Bela Sarmento-Ribeiro, Marta Pineiro, Maria Filomena Botelho, Teresa M.V.D. Pinho e Melo

PII: S0223-5234(20)30439-6

DOI: https://doi.org/10.1016/j.ejmech.2020.112468

Reference: EJMECH 112468

To appear in: *European Journal of Medicinal Chemistry*

Received Date: 7 April 2020

Revised Date: 12 May 2020

Accepted Date: 13 May 2020

Please cite this article as: M. Laranjo, Má.Campos. Aguiar, N.A.M. Pereira, Gonç. Brites, B.F.O. Nascimento, A. Brito, Joã. Casalta-Lopes, A.C. Gonçalves, A.B. Sarmento-Ribeiro, M. Pineiro, M.F. Botelho, T.M.V.D. Pinho e Melo, Platinum(II) ring-fused chlorins as efficient theranostic agents: Dyes for tumor-imaging and photodynamic therapy of cancer, *European Journal of Medicinal Chemistry* (2020), doi: https://doi.org/10.1016/j.ejmech.2020.112468.

Platinum(II) Ring-Fused Chlorins as Efficient Theranostic Agents: Dyes for Tumor-Imaging and Photodynamic Therapy of Cancer

Mafalda Laranjo,[1,2,3] Márcia Campos Aguiar,[1,4] Nelson A. M. Pereira,[4] Gonçalo Brites,[1] Bruno F. O. Nascimento,[4] Ana Brito,[1] João Casalta-Lopes,[1,5] Ana Cristina Gonçalves,[6] Ana Bela Sarmento-Ribeiro,[6] Marta Pineiro,[4] Maria Filomena Botelho,[1,2,3] and Teresa M. V. D. Pinho e Melo[4,*]

[1] University of Coimbra, Institute of Biophysics and Institute for Clinical and Biomedical Research (iCBR), area of Environment Genetics and Oncobiology (CIMAGO), Faculty of Medicine, Portugal
[2]University of Coimbra, Center for Innovative Biomedicine and Biotechnology (CIBB), Portugal
[3] University of Coimbra, Clinical and Academic Centre of Coimbra, Portugal
[4]University of Coimbra, Coimbra Chemistry Centre and Department of Chemistry, 3004-535 Coimbra, Portugal
[5]Coimbra Hospital and Universitary Centre, Radiation Oncology Service, Coimbra, Portugal
[6]University of Coimbra, Laboratory of Oncobiology and Hematology and Institute for Clinical and Biomedical Research (iCBR), area of Environment Genetics and Oncobiology (CIMAGO), Faculty of Medicine, Portugal

*tmelo@ci.uc.pt

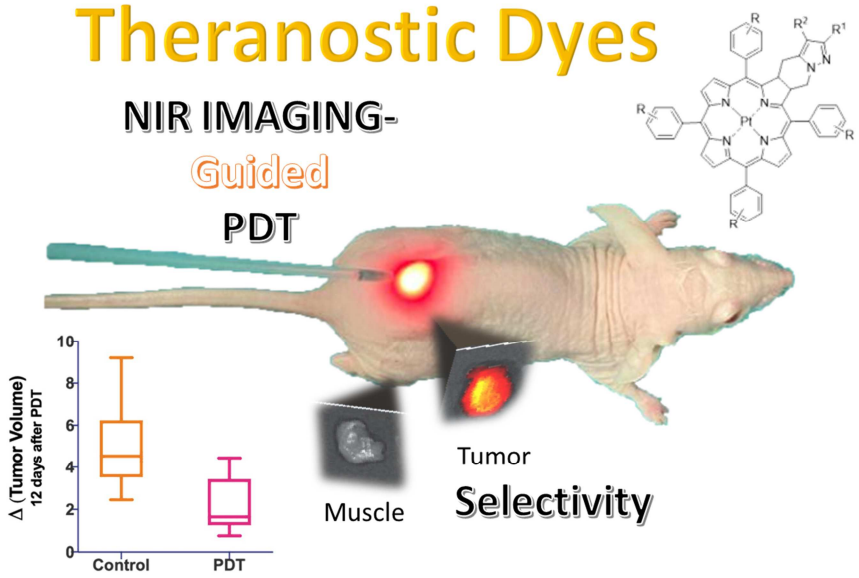

ABSTRACT

The discovery of Pt-chlorin-type theranostic agents is described. Luminescent Pt(II) 4,5,6,7-tetrahydropyrazolo[1,5-*a*]pyridine-fused chlorins, with different degrees of hydrophilicity, have been synthesized and their *in vitro* photocytotoxicity against human melanoma, oesophageal and bladder carcinomas was studied. A di(hydroxymethyl)-substituted chlorin was identified as a privileged molecule to explore imaging-guided photodynamic therapy. In addition to the high activity as PDT agent and absence of cytotoxicity *per se*, this molecule showed the ideal photophysical and photochemical properties. *In vivo* studies using a A375

melanoma mouse model, proved the extraordinary properties of this chlorin as a luminescent probe and the ability to impair tumor growth, making image guided treatment and follow up a possibility.

KEYWORDS

Pt(II) Chlorins, Photosensitizers, Photodynamic Therapy, Theranostics, Optical imaging, Luminescence imaging, Animal models, Melanoma, Bladder carcinoma, Esophageal carcinoma.

INTRODUCTION

Photodynamic therapy (PDT) has been used in the treatment of several types of cancer.[1] This therapy, based in the administration of a photosensitizer and further irradiation with visible light, elicits tumor cell death mainly by generation of reactive oxygen species (ROS) in the tumor cells. Thus, PDT is minimally invasive with selective action on tumor tissue making it a particularly interesting therapeutic approach for oncologic diseases. Furthermore, light as controllable exogenous stimulus can activate specific processes including other therapies such as chemotherapies and immunotherapies which may contribute to complete remission and cure of cancer.[2,3]

In PDT, light deep-tissue penetration is of major relevance to ensure an efficient photoactivation of the photosensitizer (PS) inside the tumor. Thus, PS molecules should absorb strongly within the phototherapeutic window, from 600 to 800 nm wavelengths, light which bears enough energy to produce ROS, can reach deeper into the tissues and avoids excitation of endogenous chromophores.[4,5]

Chlorins (dihydroporphyrins) are efficient porphyrin-derived PSs activated by the biologically friendly near-infrared (NIR) light. Among these macrocycles, either currently approved or in clinical trials, *m*-tetrahydroxyphenylchlorin (Temoporfin or Foscan), a benzoporphyrin (Verteporfin) and Radachlorin (mixture of sodium salts of chlorin e6, chlorin p6 and purpurine) stand out.[6-15]

Porphyrin-type photosensitizers developed by our group, a new type of stable 4,5,6,7-tetrahydropyrazolo[1,5-*a*]pyridine-fused chlorins obtained via [8π+2π] cycloaddition of diazafulvenium methides with porphyrins, proved to be very active photodynamic agents against several types of cancer, particularly against melanoma (Figure 1).[16-19]

Theranostics, which is the integration of imaging and therapy in a single system, allows simultaneous image-guided therapy and follow-up of the treatment outcome at an early stage, making it possible to increase treatment efficiency.[20] The development of new theranostic agents is a challenging and demanding research goal since it requires the development of biological active molecules with the necessary properties for imaging. Nevertheless, it was recently demonstrated that the incorporation of the platinum (II) into the structure of 4,5,6,7-tetrahydropyrazolo[1,5-a]pyridine-fused chlorins leads to molecules with features of

theranostic agents.[16] These compounds showed good light emission (fluorescence and phosphorescence), in solution at room temperature, in the biologically important 700-850 nm near-infrared spectral region. They have a high thermal and photochemical stability, with the phosphorescence strongly quenched by oxygen, which makes them excellent materials for use in biological imaging and act as oxygen sensors.[16]

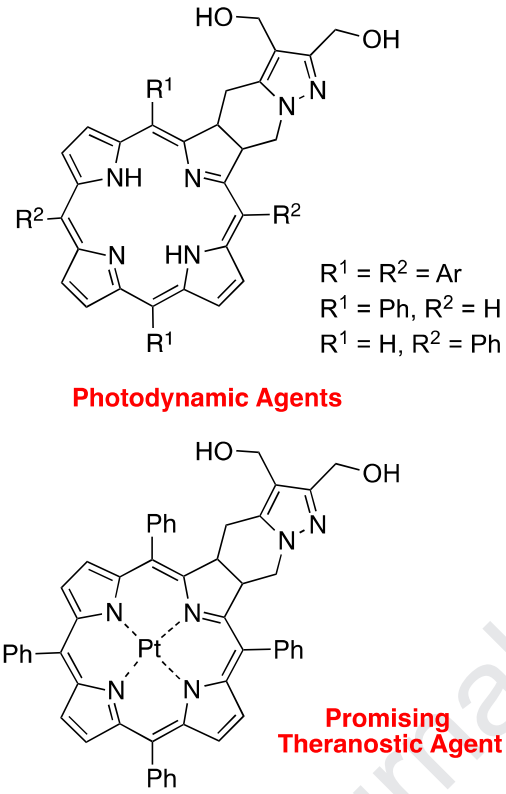

Figure 1. Chemical structures of 4,5,6,7-tetrahydropyrazolo[1,5-*a*]pyridine-fused chlorins.

Herein, further studies on near-infrared luminescent Pt(II) 4,5,6,7-tetrahydropyrazolo[1,5-*a*]pyridine-fused chlorins are described. The synthesis of a set of platinum chlorins was carried out and *in vitro* photodynamic therapy outcome against human melanoma, esophageal adenocarcinoma and bladder carcinoma cell lines was explored. Furthermore, the proof of concept of fluorescence imaging diagnostic and photodynamic treatment with the lead photosensitizer of the series, using an *in vivo* melanoma mouse model is disclosed. Biodistribution and pharmacokinetics using its intrinsic bioluminescent properties are also reported.

RESULTS AND DISCUSSION

Synthesis of Platinum (II) Ring-fused Chlorins

Platinum(II) 4,5,6,7-tetrahydropyrazolo[1,5-*a*]pyridine-fused chlorins with phenyl, 4-chlorophenyl and 4-methoxyphenyl substituents at the *meso* positions were synthetized using

the previously described strategy.[16] The phenyl, 4-chlorophenyl and 4-methoxyphenyl porphyrins **1a-c** were obtained using acid acetic/nitrobenzene as solvent and oxidant in 20, 33 and 31 % yield, respectively.[21] The corresponding Platinum (II)-complexes **2a-c** were obtained in high yields through microwave-induced metalation, using $PtCl_2$ as the metal source. The chlorin core was obtained by [8π+2π] cycloaddition of the Pt(II)-complexes **2** with the 1,7-dipole diazafulvenium methide, generated *in situ* from dimethyl 2,2-dioxo-1*H*,3*H*-pyrazolo[1,5-*c*][1,3]thiazole-6,7-dicarboxylate through thermal SO_2 extrusion, under microwave irradiation.

The modulation of the hydrophilicity of the Pt(II) chlorins was achieved through reduction of the methoxycarbonyl substituents of chlorins **3a-c** into hydroxymethyl groups and base-promoted hydrolysis of the esters into the corresponding carboxylic acid groups. The dicarboxylic derivatives **4a-c** were obtained by carrying out the hydrolysis with aqueous KOH in THF at room temperature leading to the target compounds in yields ranging from 61 to 88%. The optimized reduction conditions previously described for the synthesis of chlorin **5a**, using $LiAlH_4$ as reducing agent, were applied in the preparation of di(hydroxymethyl)-substituted chlorins **5b-c** (Scheme 1).

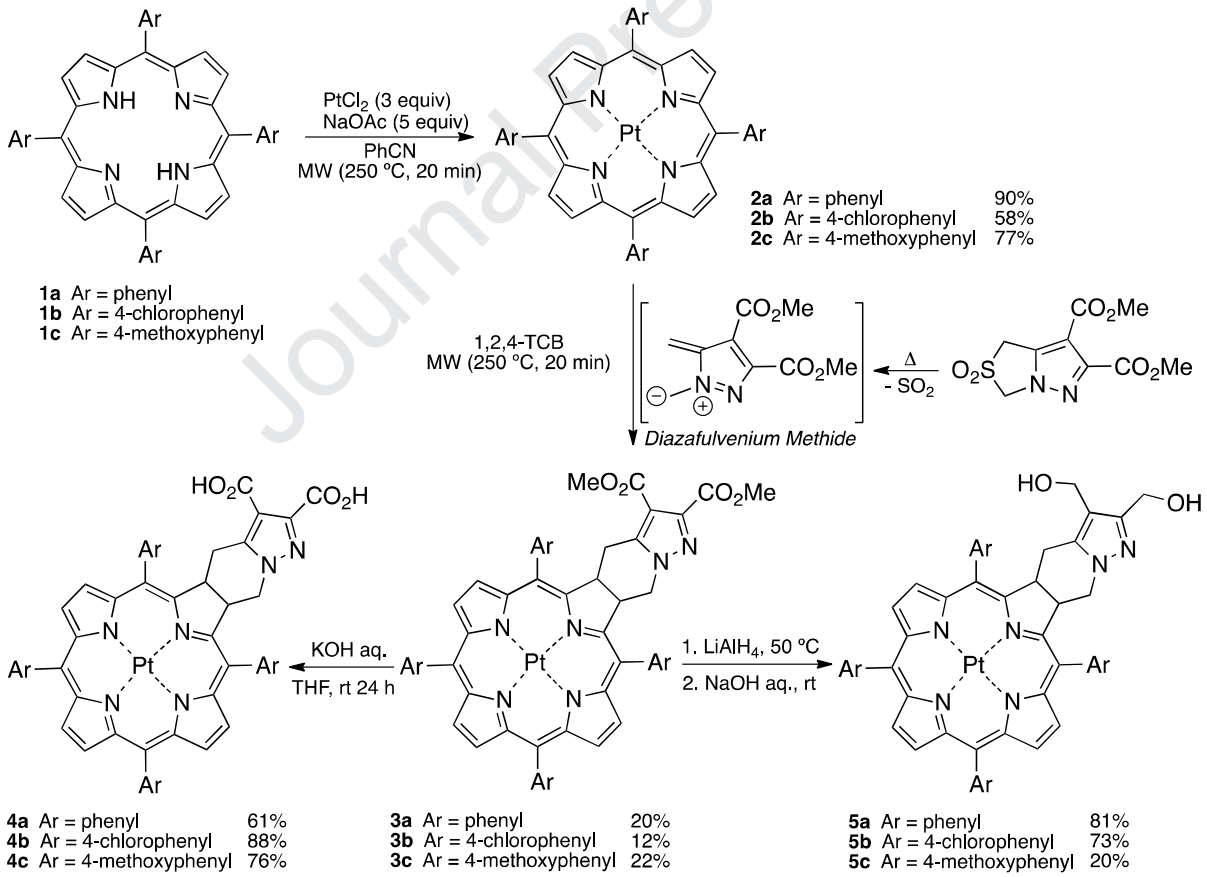

Scheme 1. Synthesis of chlorins with methoxycarbonyl **3a-c**, carboxylic **4a-c** and hydroxymethyl **5a-c** substituents.

The synthetized Pt(II)-macrocycles show the characteristic absorption spectra of chlorin derivatives, with the Soret band around 400 nm and the Q band at the higher wavelength around 590 nm. The higher hydrophilicity of hydroxymethyl and dicarboxylic acid chlorin derivatives allows their solubilization at low concentrations in PBS solutions allowing to overcome the severe aggregation problems observed for the diester derivatives **3** (see SI). Aggregation dramatically reduces singlet oxygen generation capacity decreasing the photodynamic efficiency of the sensitizer. Therefore, the cytotoxicity studies were performed with chlorins **4** and **5** bearing the carboxylic acid and hydroxymethyl substituents, respectively.

Chlorins 4a and 5a are the Most Photocytotoxic

The photocytotoxicity of chlorins **3a-c**, **4a-c** and **5a-c** against bladder carcinoma (HT1376), esophageal carcinoma (OE19) and melanocytic melanoma (A375) cell lines are presented in Figure 2. The experimental results were adjusted to sigmoid dose-response curves allowing to calculate the IC_{50} values and the respective 95% confidence intervals, being shown in the Table 1.

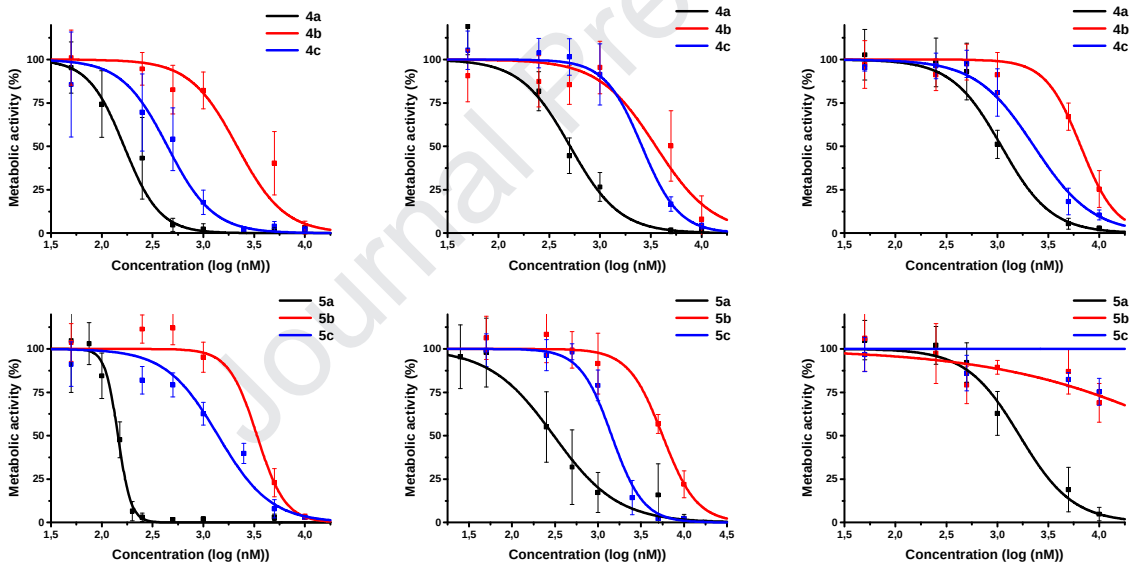

Figure 2. Sigmoid dose-response curves for chlorins **4a-c** and **5a-c** against melanoma A375 (left), oesophageal carcinoma OE19 (middle) and bladder carcinoma HT-1376 (right) cells. The analysis was performed 24 hours after PDT (irradiation wavelength > 500 nm). Data points represent mean±SD. Experimental results of chlorin **5a** against A375 cells are as previously reported.[2]

Table 1. IC_{50} levels of chlorin **4a-c** and **5a-c** in melanoma (A375) cell lines, oesophageal carcinoma (OE19) and human bladder carcinoma (HT1376).*

Chlorin	**A375 cells** $IC_{50} \pm CI_{95\%}$ **(nM)**		**OE19 cells** $IC_{50} \pm CI_{95\%}$ **(nM)**		**HT136 cells** $IC_{50} \pm CI_{95\%}$ **(nM)**	
3a-c	> 10 000		> 10 000		> 10 000	
4a	**166**	[77; 357]	**508**	[322; 802]	**1098**	[797; 1513]
4b	2149	[1041; 4437]	3551	[1180; 10 683]	6595	[5455; 8436]
4c	433	[182; 1083]	2599	[1854; 3616]	2300	[889; 5950]

5a	**144**	[122; 171]**	**306**	[167; 560]	**1657**	[1147; 2396]
5b	3376	[1568; 7271]	5644	[5089; 6259]	> 10 000	
5c	1397	[892; 2188]	1443	[744; 2799]	> 10 000	

*irradiation wavelength > 500 nm ** as previously reported.[2]

Diester-substituted chlorins **3a-c** did not present significant photocytotoxic activity. As expected, the more polar compounds, with carboxylic acid or hydroxyl substituents, prove to be more potent. The more active chlorin bearing carboxylic acid substituents was chlorin **4a**, with IC_{50} values of 1098 nM in bladder carcinoma cell line, 508 nM in oesophageal carcinoma cell line and 166 nM against melanoma cell line. Nevertheless, the most active compound was di(hydroxymethyl)-substituted chlorin **5a** with the lowest IC_{50} values against the oesophageal carcinoma cell line (IC_{50} = 306 nM) and, as previously reported, an IC_{50} value of 144 nM against the melanoma cell line.[16] Chlorin **5a** was also particularly active against bladder carcinoma cell line (IC_{50} = 1657 nM).

In previous studies, we observed that the free base chlorin, corresponding to platinum chlorin **5a**, was very active against melanoma A375 cells showing an IC_{50} value of only 31 nM as well as against another human melanoma cells (C32) with IC_{50} = 231 nM.[18] The results obtained on Pt(II)-di(hydroxymethyl)-substituted chlorin **5a** are indicative that the presence of the platinum ion does not impair photocytotoxicity since IC_{50} values in the nano-molar range were still observed. Moreover, the incorporation of this high atomic number metal ion allows for room temperature phosphorescence within the biological spectral window making these Pt(II)-ring-fused chlorins particularly interesting dyes to be used as theranostic agents.

In addition to the high activity and suitable photophysical and photochemical properties, chlorins **4a** and **5a** did not show significant cytotoxicity *per se*, that is, in the absence of light activation, not only in the human cancer cell lines but also in the human no-malignant human fibroblast HFF-1 cells (see Supporting Information, Figure S12).

These exciting results justified further studies on the mechanism of action of the more active compounds in the human melanoma A375 cell line.

Chlorins 4a and 5a Photocytotoxicity is Mainly Mediated by Singlet Oxygen

Type I photodynamic reaction results in the production ROS such as superoxide, hydrogen peroxide and hydroxyl radical through oxidation of biomolecules while in the type II reaction there is production of singlet oxygen, considered the most deleterious species in PDT.[22] To evaluate the contribution of singlet oxygen in the chlorins **4a** and **5a** (singlet oxygen quantum yield = 0.58)[16] mediated PDT, photocytotoxicity studies were carried in the presence of a quencher of this species.[23] As can be observed in Figure 3A, there is a significant impairment of photocytotoxicity of both chlorins **4a** and **5a** ($p<0.01$) in the presence of sodium azide. This evidences the preponderance of singlet oxygen generation in chlorins **4a** and **5a** mediated PDT and, therefore, the ability of these photosensitizers to elicit the type II photodynamic reaction.

Photocytotoxicity of chlorins **4a** and **5a** in the presence of hydroxyl radical scavenger was also evaluated. Figure 3B shows that the presence of this inhibitor did not influence the observed photocytotoxicity of chlorin **4a** but there was some impairment in the case of chlorin **5a** ($p<0.05$). Intracellular concentration of superoxide anion was slightly imbalanced, particularly with chlorin **4a** ($p<0.05$) and in the highest concentration of chlorin **5a** ($p = 0.003$) (Figure 3C).

Regarding peroxides (Figure 3D), PDT induced decrease of the intracellular concentration of this species with both chlorin **5a** and chlorin **4a**. In the case of chlorin **5a** this effect was already observed at concentrations equal or superior to 50 nM. This data shows that not only singlet oxygen but also type I photodynamic reaction ROS are involved in chlorin **4a** and **5a** mediated PDT.

Reduced glutathione is an antioxidant enzyme capable of eliminating free radicals and reducing peroxides.[24] As can be observed in Figure 3E, this defense was not significantly altered in response to the photodynamic treatment.

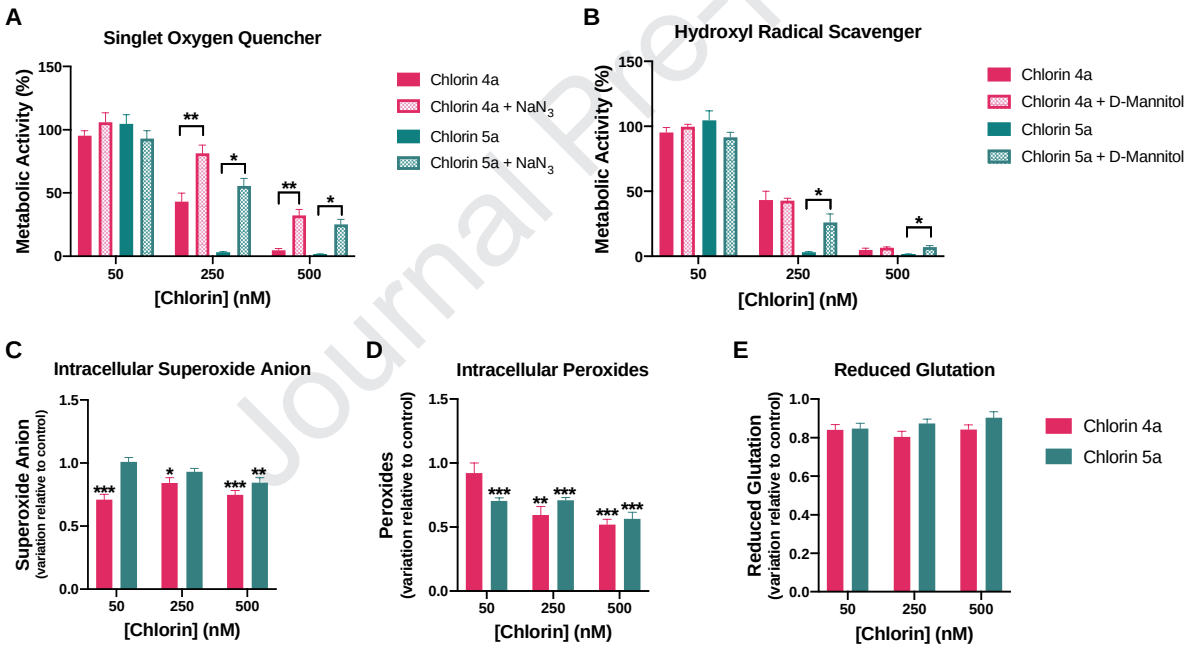

Figure 3. Photocytotoxicity of chlorins **4a** and **5a** in the human melanoma A375 cells in the presence of a singlet oxygen quencher (A) and of a hydroxyl radical scavenger (B). Significant differences relative to cell cultures treated in the absence of the inhibitors are presented with an *. Intracellular production of ROS, namely superoxide anion (C) and peroxides (D), and variation of reduced glutathione (E) in the human melanoma A375 cells after PDT. The analyses were carried out 24 hours after PDT. Results are presented as mean±SE. Statistical significance: *$p<0.05$; **$p<0.01$; ***$p<0.001$.

Chlorin 5a-mediated PDT Induces Cell Death Associated with Disruption of Mitochondrial Membrane Potential

The populations of cells in death by apoptosis, late apoptosis and necrosis are influenced by the photodynamic treatment with the photosensitizers **4a** and **5a**, as shown in the Figure 4A.

24 hours after PDT with chlorin **4a**, significant reduction of living cells was observed, to 75.33±8.21% (p=0.036) at 250 nM and to 42.17±10.28% (p<0.001) at 500 nM. Concomitantly, there was a significant increase in apoptosis cells to 11.00±3.63% (p<0.001) at 250 nM while a significant increase of death by late apoptosis (6.00±1.79%, p=0.001) and by necrosis (45.00±12.92%, p=0.001) was seen at 500 nM. In a similar manner, chlorin **5a**-mediated PDT led to a significant reduction of the viability to 77.83±10.57% (p=0.048; 250 nM) and to 63.67±11.81% (p<0.001; 500 nM solution). Regarding the type of cell death, a significant increase of apoptosis (to 7.667±2.16%, p=0.003, 50 nM), late apoptosis (8.83±3.87%, p=0.006, 250 nM) and necrosis (27.33±10.75%, p=0.002, 500 nM) were observed.

Although both apoptosis and necrosis were initiated as consequence of chlorin **4a** and **5a** based PDT, the onset of necrosis is observed preferentially with the higher concentrations. The same type of cell response was also previously observed after PDT with free base ring-fused 5,15-diphenylchlorins.[17]

It was also at the highest concentration of 500 nM that a significant disturbance of the mitochondrial membrane potential was observed after PDT with chlorin **5a** (13.66±0.50, p=0.042; see Figure 4B). The mitochondrial membrane potential reflects the mitochondrial function and the activity of the electron transport chain. Potential disruption is associated with apoptosis once it usually precedes release of cytocrom C, SMAC or AIF. Severe damage to mitochondria is also a feature of several types of regulated necrosis, which in some cases follows the generation of reactive oxygen species (ROS).[25]

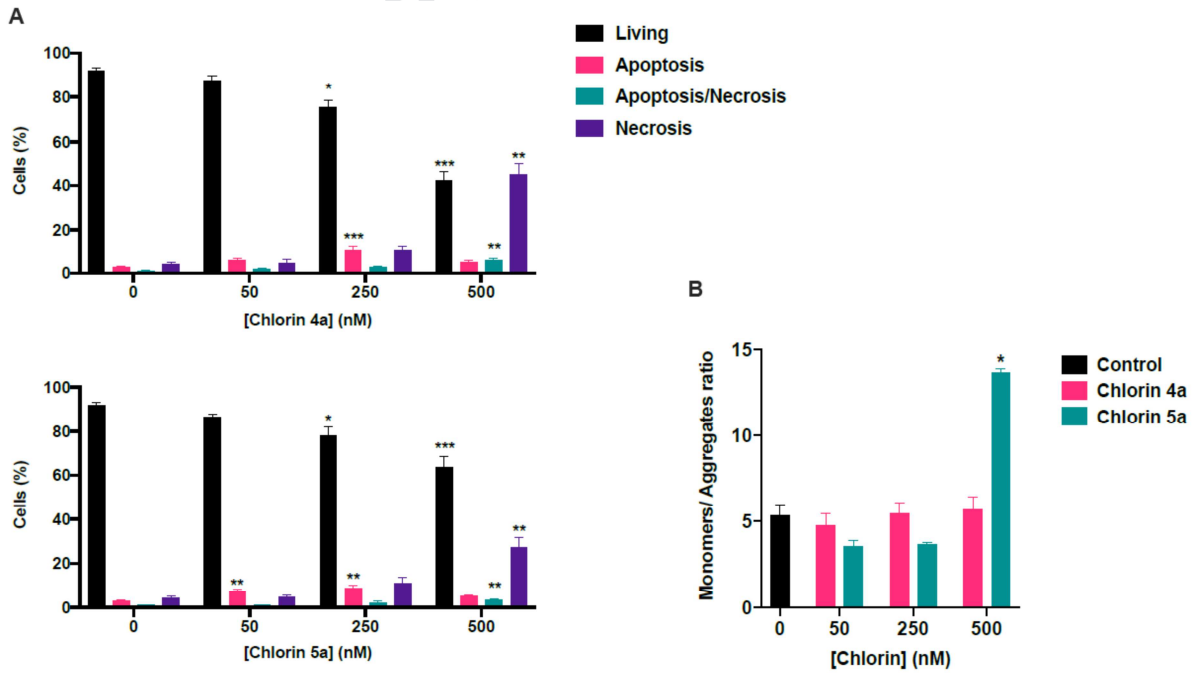

Figure 4. Types of cell death (A) and mitochondrial membrane potential (B) after PDT with the chlorins **4a** and **5a** in the human melanoma A375 cells (light dose of 10 J). Mitochondrial membrane potential is expressed as the monomer/aggregate ratio. Both analyses were carried out 24 hours after PDT. Results are presented as mean±SE. Statistical significance: *p<0.05; **p<0.01, ***p<0.001.

Chlorin 5a-Mediated PDT May Elicit a Cytostatic Effect

Cell cycle analysis shows that after PDT with chlorin **4a** (at the highest concentration of 500 nM) in human melanoma A375 cells promoted a slight decrease of the cell population in G0/G1 from 69.17±2.93% to 66.67±9.20 (p=0.033). A similar trend was observed with chlorin **5a** (500 nM) based PDT, the cell population in G0/G1 decreased to 54.17±3.66% (p<0.001) being compensated with the increase of the number of cells in S-phase (from 18.17±3.76% to 28.17±5.08%, p=0.045).

As can be observed in Figure 5, the cell cycle after photodynamic treatment with chlorins **4a** and **5a** is in line with previous studies with the free base ring-fused 5,15-diphenylchlorins[3] and *meso*-tetraarylchlorins.[18] The alterations observed at the higher concentrations, particularly with chlorin **5a**, are compatible with a cytostatic effect.

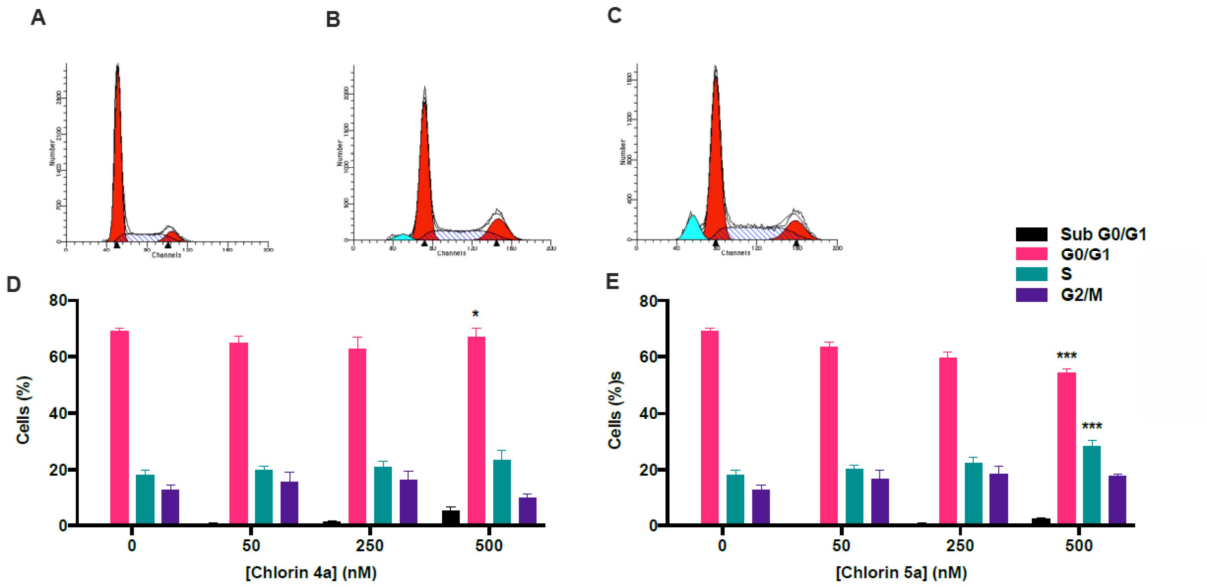

Figure 5. Cell cycle after PDT with the chlorins **4a** and **5a** in the human melanoma A375 cells (light dose of 10 J). Analysis was carried out 24 hours after PDT. Representative plots of cell cycle distribution of control cell cultures (A) and photosensitized with 500 nM chlorin **4a** (B) and **5a** (C). Results for chlorin **4a** (D) and **5a** (E) are presented as mean±SE. Statistical significance: *p<0.05; **p<0.01, ***p<0.001.

Chlorin 5a with Ideal Photophysical Properties for a Luminescence Imaging Probe

Chlorin **5a** presents absorption bands at 400, 486, 555 and 591 nm and fluorescence bands at 598 and 644 nm in aqueous micellar system (Tween80/DMSO/water (2:2:96, v/v/v). The fluorescence quantum yield in very low (Φ_F = 0.0001) and independent of the oxygen concentration while the phosphorescence quantum yield at room temperature depends quantitatively on the dissolved oxygen concentration in the solution, varying from 0.0002 in oxygen saturated solutions to 0.068 in nitrogen saturated solutions. Furthermore, the phosphorescence lifetime of **5a** changed from 11.3 μs in oxygen saturated solutions to 30.9

μs in nitrogen saturated solutions.[16] These luminescent properties makes chlorin **5a** an excellent candidate to be used as probe for *in vivo* and *ex vivo* luminescence imaging.

In vivo Chlorin 5a-based Tumor Imaging and Chlorin 5a Biodistribution: Accumulation is Maximal Seven Days After Administration

Biodistribution was assessed over the time through whole-body bioluminescence imaging of nude mice bearing a melanoma tumor in the armpit (Figure 6 and 7). In the case of the treatment group, the fluorescence images were collected after the intraperitoneal administration of 500 μL of **5a** solution in Tween80/DMSO/saline solution (2:2:96, v/v/v) with 100 μg/mL concentration. Acquisition was performed with excitation at 405 nm and a fluorescence emission filter at 695-770 nm. Exposure of mice to irradiation with 405 nm did not determine significant autofluorescence in the range of 695-770 nm, except in the abdominal area, as can be observed in Figure 7C. This emission is probably due to the contents of the intestines where molecules as the bilirubin's typical of the gastrointestinal tract and metabolites originated from mice diet and are contained, as well as, due to the hepatobiliary route of elimination of chlorin **5a**.

Figure 6B shows the images of the organs, where ROI of equal area were drawn to obtain the epifluorescence variation (that is, epifluorescence of certain organ from chlorin **5a** treated mice *vs.* epifluorescence in the same organ from untreated mice) presented in the graph of Figure 6A. At the first timepoint, 24 hours after administration, the photosensitizer accumulated preferentially in tumor, skin, liver, kidney and bladder. The initial accumulation in highly perfused organs such as liver, lung or kidneys is common due to rapid distribution in the bloodstream. In the first days after administration of the photosensitizer, the concentrations remained relatively constant in organs such as the liver, kidneys and bladder pointing to combined hepatobiliary and renal routes of excretion. In fact, chlorin **5a** presented a slow pharmacokinetics, as expectable due to the high molecular weight and the solubility properties.

The high accumulation in skin in the first 24 hours decreased gradually during the following days, probably representing a short period of photosensitivity to daylight exposure. On the contrary, concentration in the tumor and in the muscle increased, but in different proportions. The concentration in muscle increased until the fifth day and remained constant for the subsequent days. However, in the tumor the concentration increases three-fold (regarding the first 24 hours) until the seventh day, where elimination from this tissue seems to start. This kinetics determines a favorable tumor to skin and tumor to muscle ratios, seven to ten days after administration, as shown in the Figure 7A. These data points to an appropriate time to perform the therapeutic treatment from seven to ten days after sensitizer administration, where the balance between the high accumulation in tumor and low skin photosensitivity is maximized.

Chlorin 5a mediated PDT Impairs Tumor Growth in vivo

Considering biodistribution studies results, a group of tumor bearing Balb-c nu/nu mice was submitted to chlorin **5a** mediated PDT, considering a drug light interval of seven days and two drug doses, 1 mg/kg and 2 mg/kg. Figure 7B shows the relative tumor volume of the three groups of mice. The untreated control group tumors volume increased up to 5-fold during the 12 days of follow up. In treated animals the tumor development has significantly slowed down and the group where a 2 mg/kg drug dose was used only a 2-fold increase was observed 12 days after PDT. Thus, PDT with chlorin **5a** impairs tumor growth *in vivo*. This can be confirmed with the Kaplan-Meier analysis that shows significant difference regarding the probability of tumors reaching double its initial volume between the groups, animals submitted to PDT with chlorin **5a** and the untreated controls (p=0.006).

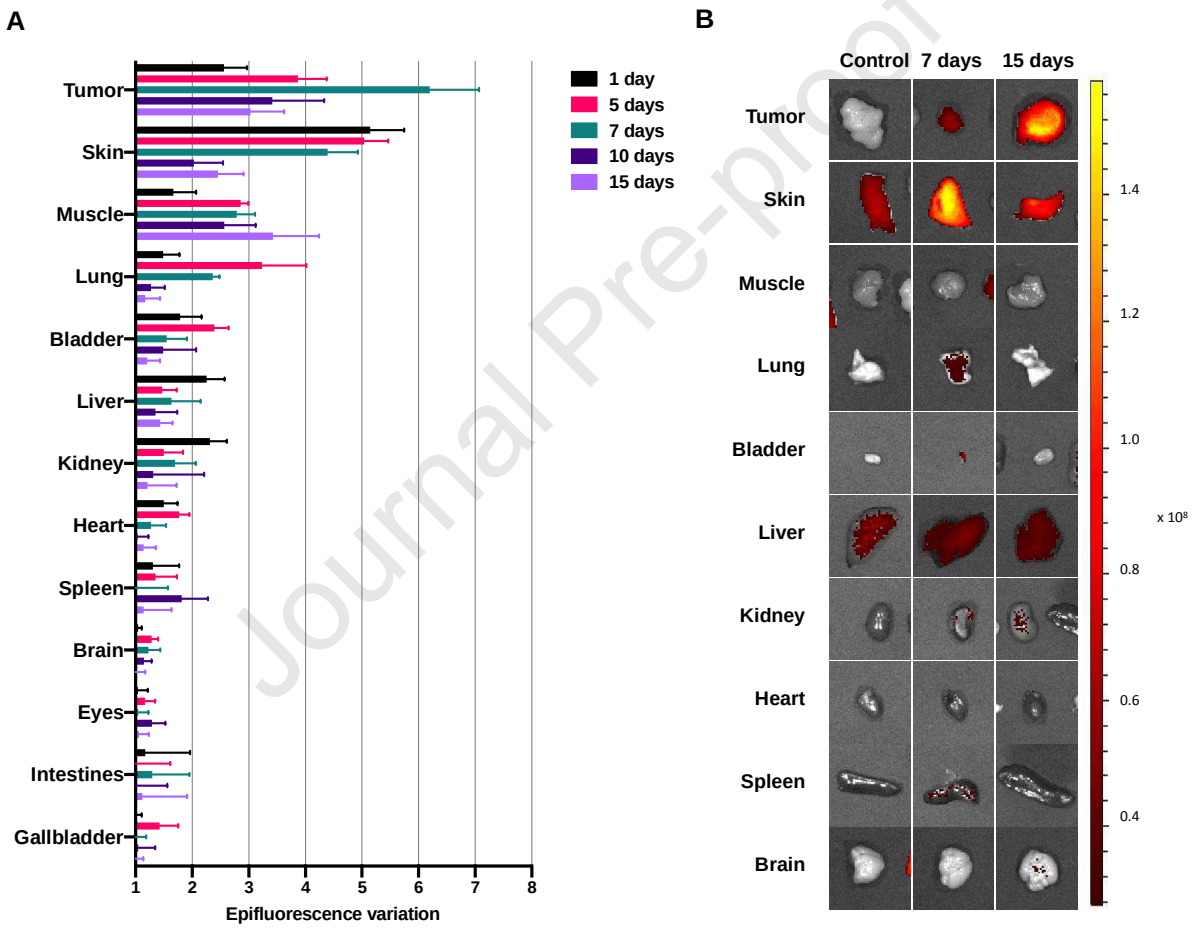

Figure 6. Biodistribution of chlorin **5a** in Balb-c nu/nu mice. The epifluorescence variation (A) corresponds to the ratio between the sum of epifluorescence intensity in a certain organ vs. the sum of epifluorescence intensity of the same organ of an animal not submitted to the photosensitizer. The values were obtained by drawing equal ROIs in the images acquired. In the image (B) are shown representative organs used to obtain the epifluorescence variation. Organ images were rearranged for illustration purposes. Full images are show in supporting information, Figure S13.

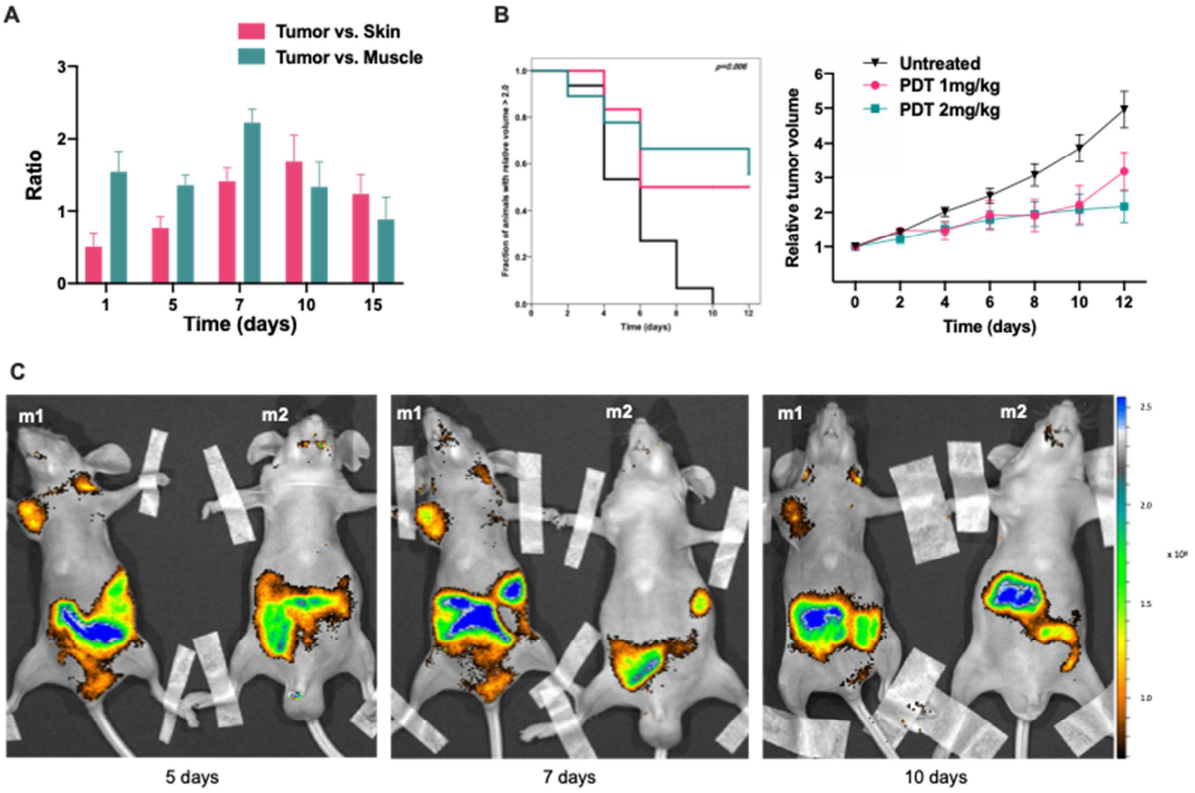

Figure 7. Tumor vs. skin and tumor vs. muscle ratio up to 15 days after chlorin **5a** administration (A). Kaplan-Meier curves of the probability of tumors not reaching two-times its initial volume, for different time points. Relative tumor volume of xenografts of animals submitted to PDT with chlorin **5a** (1 mg/kg and 2 mg/kg) compared to untreated controls (B). Representative bioluminiscence images obtained 5, 7 and 10 days after chlorin **5a** administration (C). All animais have a xenograft in the axilary region. The animal identified with ***m1*** was administered with chlorin **5a** and animal identified with ***m2*** is a control group animais not submitted to fotosensitizer. The images obtained for the same animals 1 and 15 days after administration are presented in the supporting information, Figure S14.

CONCLUSION

The synthesis of platinum(II) 4,5,6,7-tetrahydropyrazolo[1,5-*a*]pyridine-fused chlorins with different degrees of hydrophilicity have been synthesized and their evaluation as PDT agents was carried out. Among the studied photosensitizers, di(hydroxymethyl)-substituted chlorin **5a** stood out as the more promising molecule.

Chlorin **5a** proved to be a new theranostic agent to be used as luminiscence imaging probe and photosensitizer. This chlorin was active *in vitro* against human melanoma, oesophageal and bladder carcinomas, more active than the corresponding analogues where the hydroxymethyl groups were replaced by methoxycarbonyl and carboxylic acid groups. Chlorin **5a** did not show cytotoxicity *per se*, both in tumor and in fibroblast cells, showing that light is a requirement for the observed activity. This cytotoxicity, in the case of chlorin **5a**, is mediated mainly by singlet oxygen inducing cell death with mitochondrial disruption and possibly cytostatic effect. *In vivo* studies using a A375 melanoma/mouse model, proved the extraordinary properties of chlorin **5a** as a luminescent probe. The tumor-imaging and

biodistribution of chlorin **5a** allowed to establish the appropriate time to perform the therapeutic treatment, where the high accumulation in tumor and low skin photosensitizing is maximized. Irradiation of tumor-bearing mice in this time-point significantly impaired tumor growth, make image guided treatment and follow up a possibility.

EXPERIMENTAL

General experimental methods

Commercially available high-grade materials and reagents were used as received. Organic solvents were purified by standard literature procedures prior to utilization.[26] Microwave-assisted reactions were carried out with a CEM Discover S-Class focused microwave reactor featuring continuous temperature, pressure and microwave power control, under closed vessel conditions. Reaction monitoring was made by thin layer chromatography (TLC) analysis on SiO_2 60 F_{254}-coated aluminum plates and via UV-vis absorption spectroscopy, using a PG Instruments T80, Shimadzu UV-2100 or Hitachi U-2001 spectrophotometer. Flash column chromatography was performed using SiO_2 60 (35-70 µm) as the stationary phase. Melting points were determined with a FALC R132467 electrothermal apparatus, using open glass capillaries, and are uncorrected. UV-vis absorption spectra were obtained on a PG Instruments T80 or Shimadzu UV-2100 spectrophotometer using standard 1 cm-wide quartz cuvettes. Maximum wavelengths (λ) are given in nanometers. NMR spectra were recorded at room temperature with a Bruker Avance III spectrometer, operating at 400 MHz (^{1}H) and 100 MHz MHz (^{13}C). Tetramethylsilane (TMS) was used as internal standard. Chemical shifts (δ) are expressed in parts per million related to TMS and coupling constants (J) are conveyed in hertz. HRMS spectra were obtained with a Waters Micromass VG Autospec M ESI-TOF spectrometer.

Synthesis

Pt(II) porphyrin **2a-b**[27] were prepared following a literature procedure.[21] Pt(II) porphyrin **2c** was obtained similarly as a dark-purple solid in 77% yield, after purification by flash column chromatography (dichloromethane). Mp (°C) > 300; UV-vis (acetone): λ_{max} (nm) = 398, 510, 537; ^{1}H NMR (400 MHz, $CDCl_3$): δ (ppm) = 8.77 (s, 8H, β-H pyrrolic), 8.04 (d, J = 8.5 Hz, 8H, Ar), 7.24 (d, J = 8.5 Hz, 8H, Ar), 4.06 (s, 12H, OMe); ^{13}C NMR (100 MHz, $CDCl_3$): δ (ppm) = 159.4, 143.1, 134.9, 133.8, 130.6, 112.3, 55.6; HRMS (ESI): m/z = 927.2371 (found), 927.2383 (calculated for $C_{48}H_{36}N_4O_4Pt$, M^+).

Pt(II) chlorins **3a**, **3b** and **3c** were synthesized according to a synthetic approach previously described by us, under microwave irradiation.[16, 18, 28, 29] Products were isolated as a purple solids after purification by flash chromatography using CH_2Cl_2/ethyl acetate (95:5) as eluent.

Chlorin **3b** was obtained in 12% yield. Mp (°C) > 300; UV-vis (acetone): λ_{max} (nm) (relative absorbance, %) = 400 (100), 483 (6.30), 553 (7.53), 591 (30.82); ^{1}H NMR (400 MHz,

$CDCl_3$): δ (ppm) = 8.38 (s, 2H, β-H pyrrolic), 8.36 (d, J = 5.0 Hz, 1H, β-H pyrrolic), 8.35 (d, J = 5.0 Hz, 1H, β-H pyrrolic), 8.13 (d, J = 5.1 Hz, 1H, β-H pyrrolic), 8.10 (d, J = 5.1 Hz, 1H, β-H pyrrolic), 8.01-7.95 (m, 3H, Ar), 7.92-7.85 (m, 4H, Ar), 7.78-7.72 (m, 4H, Ar), 7.69-7.60 (m, 6H, Ar), 5.70-5.63 (m, 1H, reduced β-H pyrrolic), 5.38-5.31 (m, 1H, reduced β-H pyrrolic), 4.38 (dd, J = 13.6, 7.4 Hz, 1H, CH_2 from fused ring), 3.91-3.85 (m, 1H, CH_2 from fused ring), 3.89 (s, 3H, CO_2Me), 3.79 (s, 3H, CO_2Me), 3.54 (dd, J = 15.9, 6.7 Hz, 1H, CH_2 from fused ring), 2.56 (dd, J = 15.9, 10.1 Hz, 1H, CH_2 from fused ring); ^{13}C NMR (100 MHz, $CDCl_3$): δ (ppm) = 162.4, 162.0, 150.9, 148.4, 146.3, 146.1, 143.0, 142.9, 138.9, 138.8, 138.4, 138.2, 138.0, 135.8, 135.7, 135.6, 135.1, 134.5, 134.3(3), 134.3(0), 134.2(3), 134.2(0), 132.6, 132.4, 132.3, 129.2, 129.0, 128.7, 128.1, 127.6(2), 127.5(7), 127.4, 126.2, 126.1, 125.7, 125.4, 112.4, 112.2, 110.8, 52.6, 51.7, 49.0, 45.5, 43.2, 26.1; HRMS (ESI): m/z = 1153.1021 (found), 1153.1038 (calculated for $C_{53}H_{34}Cl_4N_6O_4Pt$, M^+).

Chlorin **3c** was obtained in 12% yield. Mp (°C) > 300; UV-vis (acetone): λ_{max} (nm) (relative absorbance, %) = 405 (100), 485 (5.84), 553 (8.11), 590 (30.71); ^{1}H NMR (400 MHz, $CDCl_3$): δ (ppm) = 8.44 (d, J = 5.1 Hz, 1H, β-H pyrrolic), 8.42 (d, J = 5.1 Hz, 1H, β-H pyrrolic), 8.39 (d, J = 5.1 Hz, 1H, β-H pyrrolic), 8.38 (d, J = 5.1 Hz, 1H, β-H pyrrolic), 8.16 (d, J = 5.0 Hz, 1H, β-H pyrrolic), 8.14 (d, J = 5.0 Hz, 1H, β-H pyrrolic), 7.98-7.81 (m, 8H, Ar), 7.28-7.25 (m, 2H, Ar), 7.19-7.08 (m, 6H, Ar), 5.78-5.65 (m, 1H, reduced β-H pyrrolic), 5.36-5.29 (m, 1H, reduced β-H pyrrolic), 4.42 (dd, J = 13.6, 7.8 Hz, 1H, CH_2 from fused ring), 4.09-4.04 (m, 1H, CH_2 from fused ring), 4.02 (s, 6H, OMe), 4.01 (s, 3H, OMe), 4.00 (s, 3H, OMe), 3.90 (s, 3H, CO_2Me), 3.74 (s, 3H, CO_2Me), 3.57 (dd, J = 15.9, 6.5 Hz, 1H, CH_2 from fused ring), 2.51 (dd, J = 15.9, 10.1 Hz, 1H, CH_2 from fused ring); ^{13}C NMR (100 MHz, $CDCl_3$): δ (ppm) = 162.6, 162.2, 159.6, 159.5, 159.4, 151.0, 148.6, 146.7, 146.6, 143.5, 142.9, 138.7, 138.5, 136.1, 135.9, 135.6, 135.1, 134.4, 134.3, 133.2, 132.9, 132.4, 132.3, 132.2, 132.1, 127.4(2), 127.3(8), 126.5, 126.3, 125.9(4), 125.8(6), 114.2, 113.8, 113.7, 113.3, 112.9, 112.7, 112.5, 110.7, 55.5, 55.4(4), 55.4(0), 52.6, 51.5, 49.3, 45.5, 43.3, 26.2; HRMS (ESI): m/z = 1137.3007 (found), 1137.3023 (calculated for $C_{57}H_{46}N_6O_8Pt$, M^+).

General procedure for the synthesis of Pt(II) chlorins 4

To a solution of the respective Pt(II) chlorin **3** (0.025 mmol) in THF (5 mL) was added saturated aqueous KOH (1 mL) and the reaction mixture was left stirring at room temperature overnight. After evaporation of the solvent, water (5 mL) was added to the crude product mixture, followed by cooling to 0 °C and neutralization by the careful addition of aqueous 1 M HCl. The resulting thin solid was filtered off, washed with water and then purified by flash column chromatography using CH_2Cl_2/methanol (90:10) as eluent. Pt(II) chlorins **4a-c** were obtained as purple solids.

Pt(II) chlorin **4a** was obtained in 61% yield from **3a** following the general procedure. Mp (°C) > 300; UV-vis (acetone): λ_{max} (nm) (relative absorbance, %) = 399 (100), 484 (5.51), 553 (6.74), 590 (20.23); ^{1}H NMR (400 MHz, DMSO-d_6): δ (ppm) = 8.33 (d, J = 5.0 Hz, 1H, β-H pyrrolic), 8.32 (d, J = 5.0 Hz, 1H, β-H pyrrolic), 8.30 (d, J = 5.0 Hz, 1H, β-H pyrrolic), 8.29 (d, J = 5.0 Hz, 1H, β-H pyrrolic), 8.21 (t, J = 8.1 Hz, 2H, Ar), 8.15 (d, J = 5.0 Hz, 1H, β-H pyrrolic), 8.11-8.04 (m, 2H, Ar), 8.07 (d, J = 5.0 Hz, 1H, β-H pyrrolic), 8.02 (d, J = 7.3 Hz,

2H, Ar), 7.99-7.96 (m, 2H, Ar), 7.92 (t, *J* = 7.3 Hz, 1H, Ar), 7.84-7.68 (m, 11H, Ar), 5.97-5.91 (m, 1H, reduced β-H pyrrolic), 5.61-5.55 (m, 1H, reduced β-H pyrrolic), 4.29 (dd, *J* = 13.4, 6.3 Hz, 1H, CH_2 from fused ring), 4.04 (dd, *J* = 13.4, 6.3 Hz, 1H, CH_2 from fused ring), 3.50-3.39 (m, 2H, overlapping peaks CH_2 from fused ring and H_2O); HRMS (ESI): m/z = 990.2370 (found), 990.2366 (calculated for $C_{51}H_{35}N_6O_4Pt$, $[M+H]^+$).

Pt(II) chlorin **4b** was obtained in 88% yield from **3b** following the general procedure. Mp (°C) > 300; UV-vis (nm) (acetone): λ_{max} (relative absorbance, %) = 398 (100), 483 (4.86), 554 (6.86), 591 (24.97); ^{1}H NMR (400 MHz, DMSO-d_6): δ (ppm) = 8.35 (d, *J* = 5.0 Hz, 1H, β-H pyrrolic), 8.33 (d, *J* = 5.0 Hz, 1H, β-H pyrrolic), 8.32 (d, *J* = 5.1 Hz, 1H, β-H pyrrolic), 8.31 (d, *J* = 5.1 Hz, 1H, β-H pyrrolic), 8.21 (d, *J* = 8.2 Hz, 2H, Ar), 8.14 (d, *J* = 5.1 Hz, 1H, β-H pyrrolic), 8.13-8.10 (m, 1H, Ar), 8.09 (d, *J* = 5.1 Hz, 1H, β-H pyrrolic), 8.05-7.95 (m, 6H, Ar), 7.88 (dd, *J* = 8.2, 2.3 Hz, 1H, Ar), 7.82-7.74 (m, 6H, Ar), 5.94-5.88 (m, 1H, reduced β-H pyrrolic), 5.63-5.58 (m, 1H, reduced β-H pyrrolic), 4.26 (dd, *J* = 13.6, 6.0 Hz, 1H, CH_2 from fused ring), 4.10 (dd, *J* = 13.6, 6.0 Hz, 1H, CH_2 from fused ring), 3.47-3.40 (m, 2H, overlapping peaks CH_2 from fused ring and H_2O); HRMS (ESI): m/z = 1125.0487 (found), 1125.0464 (calculated for $C_{51}H_{30}Cl_4N_6O_4Pt$, M^+).

Pt(II) chlorin **4c** was obtained in 76% yield from **3c** following the general procedure. Mp (°C) > 300; UV-vis (nm) (acetone): λ_{max} (relative absorbance, %) = 403 (100), 485 (5.75), 553 (7.45), 590 (25.44); ^{1}H NMR (400 MHz, DMSO-d_6): δ (ppm) = 8.36 (d, *J* = 5.3 Hz, 1H, β-H pyrrolic), 8.35 (d, *J* = 5.3 Hz, 1H, β-H pyrrolic), 8.32 (d, *J* = 4.9 Hz, 2H, overlapping β-H pyrrolic), 8.14 (d, *J* = 4.9 Hz, 1H, β-H pyrrolic), 8.10-8.07 (m, 1H, Ar), 8.09 (d, *J* = 4.9 Hz, 1H, β-H pyrrolic), 7.99 (d, *J* = 8.4 Hz, 1H, Ar), 7.95 (d, *J* = 7.4 Hz, 1H, Ar), 7.91-7.89 (m, 1H, Ar), 7.87-7.84 (m, 3H, Ar), 7.44-7.43 (m, 1H, Ar), 7.36 (dd, *J* = 8.2, 2.1 Hz, 1H, Ar), 7.29-7.18 (m, 7H, Ar), 5.94-5.84 (m, 1H, reduced β-H pyrrolic), 5.58-5.52 (m, 1H, reduced β-H pyrrolic), 4.29-4.23 (m, 1H, CH_2 from fused ring), 4.02-4.00 (m, 1H, CH_2 from fused ring), 3.99 (s, 3H, OMe), 3.98 (s, 3H, OMe), 3.97 (s, 6H, OMe), 3.50-3.45 (m, 2H, overlapping peaks CH_2 from fused ring and H_2O); HRMS (ESI): m/z = 1109.2720 (found), 1109.2710 (calculated for $C_{55}H_{42}N_6O_8Pt$, M^+).

Pt(II) chlorins **5b** and **5c** were prepared following a procedure similar to that previously reported for **5a**[2] and were obtained as purple solids after being purified by flash column chromatography [ethyl acetate/methanol (95:5)]).

Pt(II) chlorin **5b** was obtained in 73% yield from **3b** (reaction time: 5 h). Mp (°C) > 300; UV-vis (acetone): λ_{max} (nm) (relative absorbance, %) = 399 (100), 484 (6.01), 554 (7.68), 592 (27.51); ^{1}H NMR (400 MHz, $CDCl_3$): δ (ppm) = 8.32 (d, *J* = 5.1 Hz, 1H, β-H pyrrolic), 8.30 (s, 2H, β-H pyrrolic), 8.29 (d, *J* = 5.1 Hz, 1H, β-H pyrrolic), 8.11 (d, *J* = 5.0 Hz, 1H, β-H pyrrolic), 8.06 (d, *J* = 5.0 Hz, 1H, β-H pyrrolic), 7.91 (d, *J* = 8.2 Hz, 2H, Ar), 7.87-7.78 (m, 5H, Ar), 7.70 (dd, *J* = 8.2, 2.1 Hz, 1H, Ar), 7.67 (dd, *J* = 8.2, 2.1 Hz, 2H, Ar), 7.60-7.57 (m, 5H, Ar), 7.54 (dd, *J* = 8.2, 2.1 Hz, 1H, Ar), 5.61-5.54 (m, 1H, reduced β-H pyrrolic), 5.28-5.21 (m, 1H, reduced β-H pyrrolic), 4.43-4.34 (m, 2H, CH_2OH), 4.17-4.09 (m, 2H, CH_2OH), 4.11-4.05 (m, 1H, CH_2 from fused ring), 3.80 (dd, *J* = 13.3, 9.0 Hz, 1H, CH_2 from fused

ring), 2.85 (dd, *J* = 15.4, 6.4 Hz, 1H, CH_2 from fused ring), 2.41 (dd, *J* = 15.4, 9.6 Hz, 1H, CH_2 from fused ring); ^{13}C NMR (100 MHz, $CDCl_3$): δ (ppm) = 151.6, 149.5, 149.4, 146.1, 146.0, 138.9(1), 138.8(7), 138.6, 138.0, 137.8, 137.4, 135.7, 135.5, 135.2, 134.8, 134.5, 134.4, 134.2, 132.7, 132.6, 132.3, 132.2, 129.0, 128.9, 128.4, 127.9, 127.4, 127.3, 126.1, 126.0, 125.4, 125.2, 114.9, 112.3, 112.0, 57.4, 53.9, 48.3, 45.8, 44.0, 24.9; HRMS (ESI): m/z = 1097.1165 (found), 1097.1140 (calculated for $C_{51}H_{34}Cl_4N_6O_2Pt$, M^+).

Pt(II) chlorin **5c** was obtained in 20% yield from **3c** (reaction time: 32 h). Mp (°C) > 300; UV-vis (acetone): λ_{max} (relative absorbance, %) = 403 (100), 485 (6.67), 554 (8.74), 589 (24.05); ^{1}H NMR (400 MHz, $CDCl_3$): δ (ppm) = 8.42 (s, 2H, β-H pyrrolic), 8.39 (d, *J* = 5.0 Hz, 1H, β-H pyrrolic), 8.37 (d, *J* = 5.0 Hz, 1H, β-H pyrrolic), 8.16 (d, *J* = 5.0 Hz, 1H, β-H pyrrolic), 8.13 (d, *J* = 5.0 Hz, 1H, β-H pyrrolic), 7.95 (dd, *J* = 8.3, 2.2 Hz, 2H, Ar), 7.89-7.86 (m, 3H, Ar), 7.81 (dd, *J* = 8.3, 2.2 Hz, 1H, Ar), 7.66 (dd, *J* = 8.3, 2.2 Hz, 1H, Ar), 7.23 (dd, *J* = 8.4, 2.7 Hz, 2H, Ar), 7.20-7.15 (m, 5H, Ar), 7.12 (dd, *J* = 8.4, 2.7 Hz, 1H, Ar), 7.08 (dd, *J* = 8.4, 2.7 Hz, 1H, Ar), 5.72-5.65 (m, 1H, reduced β-H pyrrolic), 5.31-5.25 (m, 1H, reduced β-H pyrrolic), 4.56 (s, 2H, CH_2OH), 4.28-4.21 (m, 2H, CH_2OH), 4.21-4.17 (m, 1H, CH_2 from fused ring), 4.03 (s, 3H, OMe), 4.02 (s, 3H, OMe), 3.98 (s, 3H, OMe), 3.97 (s, 3H, OMe), 3.92 (dd, *J* = 8.7, 4.7 Hz, 1H, CH_2 from fused ring), 2.95 (dd, *J* = 15.3, 6.4 Hz, 1H, CH_2 from fused ring), 2.46 (dd, *J* = 15.3, 10.1 Hz, 1H, CH_2 from fused ring); HRMS (ESI): m/z = 1081.3156 (found), 1081.3121 (calculated for $C_{55}H_{46}N_6O_6Pt$, M^+).

Cell culture conditions

Bladder carcinoma cell line HT1376 and melanoma cell line A375 were obtained from the American Type Culture Collection (ATCC, CRL-1472 and CRL-1619, respectively). The esophageal carcinoma cell line is designated OE19 and was obtained from the European Collection of Cell Cultures (ECACC, JROECL19). The cell lines were cultured according to the supplier's recommendations. The HT1376 and the A375 cell lines were cultured in Dulbecco's Modified Eagle medium (Sigma-Aldrich, Inc; Sigma D-5648) supplemented with 10% heat-inactivated fetal bovine serum (Gibco Invitrogen Life Technologies; Gibco 2010-04), 1% Penicillin–Streptomycin (Gibco Invitrogen Life Technologies; 100U/mL penicillin and 10 μg/mL streptomycin – Gibco 15140-122) and 100 μM sodium pyruvate (Gibco Invitrogen Life Technologies; Gibco 1360). The OE19 cell line was cultured in Roswell Park Memorial Institute 1640 medium (RPMI 1640, Sigma R4130), supplemented with 10% heat-inactivated fetal bovine serum (FBS, Sigma F7524), 1% penicillin-streptomycin (100 U/mL penicillin and 10 mg/mL streptomycin, Gibco 15140-122), and 400 mM sodium pyruvate (Gibco Invitrogen Life Technologies; Gibco 1360). All cell lines were kept at 37 ºC, in a humidified incubator with 95% air and 5% CO_2. For all studies, cells were detached using a solution of 0.25% trypsin-EDTA (Gibco).

Photodynamic treatment *in vitro*

For each experiment, A375 cells were plated and kept in the incubator overnight, in order to allow the attachment of the cells. The initial formulation of the sensitizers consisted of a 1mg/mL solution in DMSO and the desired concentrations were achieved by successive dilutions, being always administered to the cells at 1% DMSO. After sensitizer

administration (from 1 nM to 10 μM), cells were incubated for 24 h. Controls were performed on every test. Cells were washed with PBS and new drug-free medium was added. Each plate was irradiated with a fluence rate of 7.5 mW/cm^2 until a total of 10 J was reached, using a fluorescent light source equipped with a red filter (cut off < 560 nm). Analysis were performed 24 hours after photodynamic treatment.

Photocytotoxicity and cytotoxicity

To the evaluation of photocytotoxicity to the chlorins, an MTT assay to evaluate metabolic activity was performed. To the evaluation of cytotoxicity of the chlorins, cell cultures were submitted to the same procedure described above, omitting the irradiation step.

Cell culture plates were washed and incubated with a solution of 3-(4,5-dimethylthiazol-2-yl)-2,5-diphenyltetrazolium bromide (0.5mg/mL, Sigma) in PBS, pH 7.4, in the dark at 37 °C for 4 hours. To solubilize formazan crystals, a 0.04 M solution of hydrochloric acid in isopropanol was added. Absorbance was measured using an Biotek Synergy HT Plate Reader. Each experiment was performed in triplicate and repeated in three sets of tests

Results allowed to establish dose-response curves, using Origin 8.0 software, and to calculate the concentration of sensitizers that inhibits the proliferation of cultures in 50% (IC50).

Types of cell death

For this and the subsequent studies the A375 cell cultures were used, being submitted to the photodynamic treatment based on the chlorins **4a** and **5a** in the concentrations of 50 nM, 250 nM and 500 nM. Cell viability was assessed using annexin-V and propidium iodide incorporation. Cells were labelled with fluorescein isothiocyanate conjugate annexin-V (an-V) and propidium iodide (PI) as described by the supplier (Immunostep, ANXVIKF-100T). Cells were analyzed in a four-color FACSCalibur flow cytometer (Becton Dickinson) and processed in the Paint-A-Gate software (Becton Dickinson). Results are expressed in percentage of apoptotic (an-V+/PI), late apoptotic/necrotic (an-V+/PI+), necrotic (an-V-/PI+) and viable cells (an-V-/PI-).

Mitochondrial membrane potential

The fluorescent probe, JC-1 (1st J-aggregate-forming cationic; 5,50,6,60-tetrachloro-1,10,3,30-tetraethylbenzi-midazol carbocyanine, JC-1, T4069, Sigma-Aldrich), was used to label the cells during 15 minutes, at 37°C, in the dark, prior flow cytometry evaluation. The results are presented as the monomers/aggregates (M/A) ratio, which is inversely proportional to the mitochondrial membrane potential.

Cell cycle analysis

Cells were fixed in ethanol 70% (Sigma 24102) at 4 °C for 30 minutes, washed, and incubated with the PI/RNase solution (PI/RNase, Immunostep) for 15 minutes, as recommended by the kit manufacturer. Samples were analysed in the FACSCalibur and processed in the Mod-fit software.

Photocytotoxicity in the presence of ROS inhibitors

Cells were plated and the sensitizers were administered in the same conditions described above. After 24 hours of incubation, respectively, cells were washed with PBS and medium with ROS inhibitors was added: NaN_3 (5mM, Sigma 71290) as a singlet oxygen quencher and D-mannitol (40 mM, Sigma M4125) as a hydroxyl radical scavenger. The cell cultures were incubated for 2 hours and then irradiated under the same conditions as described in the previous section. After irradiation, the cell cultures were incubated for 30 minutes and then new photosensitizer-drug, free-ROS inhibitors medium was added. Cell line sensitivity to PDT in these conditions was evaluated using MTT assay as described above.

Intracellular production of ROS

Production of intracellular peroxides was determined by incubation of 5 μM of 2′,7′-dichlorodihydrofluorescein diacetate (DCFH2-DA, Invitrogen Life technologies, D399) probe, for 45 minutes in the dark at 37 °C. The production of superoxide anion was evaluated using 2μM dihydroethidium (DHE, Sigma D7008) probe, incubated during 10 minutes with the cells, at room temperature in the dark. Analysis was performed by flow cytometry.

Reduced glutathione

Detection of the expression of intracellular reduced glutathione (GSH), was performed using 40μM of mercury orange (Sigma M7750), which was left during 15 minutes of incubation, at 37 °C in the dark. Samples were analyzed by flow cytometry.

Animal studies

All animal studies were performed according to the Regulation of the Animal Welfare Authority of the Animal Science Faculty of the Institute of Clinical and Biomedical Research of Coimbra, Faculty of Medicine, University of Coimbra (Approved ID: ORBEA 26-2015) and the European Union law. The project was approved by the Direção Geral de Alimentação e Veterinária (General Direction of Food and Veterinary, Portugal, Process 010602 of April 29th, 2016).

Eighth-weeks-old athymic nude mice (Balb/c nu/nu) were used. Animal housing was performed in individually ventilated boxes, with litter, enrichment and nesting material. Food and water were provided *ad libitum*.

Fluorescence imaging and biodistribution

The Balb-c nu/nu mice were inoculated with $5x10^6$ human melanoma A375 cells in the axillary region. When a palpable tumor mass was present the studies were initiated. The animals were divided into two groups. One group of 25 mice was administrated by intraperitoneal injection with 500 μL of 0.1 mg/mL of chlorin **5a** in Tween80/DMSO/saline solution (2:2:96, v/v/v). The other group of 10 mice was used as control, without administration of photosensitizers.

Imaging studies were performed 1, 5, 7, 10 and 15 days after injection. For this the mice were anesthetized intraperitoneally with 2 μL/g of a 3:1 ketamine and chlorpromazine solution.

Whole-body fluorescence imaging was performed in the IVIS Lumina XR optical imaging system equipped with a 150 W tungsten/halogen lamp and appropriates filters (Caliper LifeScience, Hopkinton, MA, USA), that allow to use the excitation light at 405 nm and emission filter at 695-770 nm.

For the biodistribution studies, the same animals were killed immediately after image acquisition considering the same time-points, meaning 7 mice (5 treated with the chlorin 5a and 2 from control group) were killed at day one, the same number of mice at day 5 and so on. Animals were dissected and organs collected in order to obtain fluorescence images in the IVIS Lumina XR.

All images were taken in automatic mode and are presented without change to the color scale.
Fluorescent signals were quantified using the Living Image 4.5.2. software (IVIS Imaging Systems) and are expressed in radiant efficiency ($p/s/cm^2/sr)(\mu W/cm^2$). The same region of interest (ROI) was drawn on the tumor region in both treated and untreated mice. To express the biodistribution, the epifluorescence variation was calculated as the ratio between the ROI located over a tumor in the treated vs. untreated mice, that is, the ratio between the sum of epifluorescence intensity in a certain organ *vs*. the sum of epifluorescence intensity of the same organ of an animal not submitted to the photosensitizer.

Photodynamic therapy *in vivo*

Thirty Balb-c nu/nu mice were inoculated subcutaneously with $10x10^6$ cells in the back region. Tumors were monitored daily to check its volume, considering the following expression: $V = (L \times S2)/2$, where L is the largest axis of the tumor and S the smallest axis is S.[30] When tumors reached 150-250 mm^3, the animals were divided into 3 groups, that differed in the dose of chlorin **5a** administered. One group was administered with 2mg/kg, other group with 1mg/kg and the other was used as the control without chlorin administration. After the seven days the animals were anesthetized and irradiated in the tumors area using a laser light with a power of 0.15 W until 100 J was reached (Ceramoptec Ceralas). Monitoring of tumor volume was carried out every 48 h during 12 days more days.

Statistical analysis

Statistical analysis was performed via IBM® SPSS® software, version 22.0 (IBM Corporation, ARMONK, New York, USA). The normality of the distribution of each quantitative variable was evaluated according to the Shapiro-Wilk test, with the aim of determining the use of parametric or non-parametric tests.

The normalized values (superoxide anion, peroxides and reduced glutathione) of the experimental conditions were compared with the respective normalization value using the one sample t-test. In the case of metabolic activity in the presence of the singlet oxygen quencher and hydroxyl radical scavenger the t-student test was used. The rest of the cellular studies (cell death, mitochondrial membrane potential and cell cycle) were compared with ANOVA test in cases where normal distribution and homogeneity of variances were verified

or with the Kruskal-Wallis test in the otherwise. Between some pairs of experimental groups multiple comparisons were made which were corrected using Bonferroni method. For the prospective study, the estimation of Kaplan-Meier to construct survival curves was performed considering events when tumor doubled its initial volume. The comparison of curves was performed by the Log-rank test. A significance level of 5% was considered for all comparisons.

ACKNOWLEDGMENTS

This work was funded by the Portuguese Foundation for Science and Technology (FCT) and co-funded by FEDER through COMPETE 2020 (project no. POCI-01-0145FEDER-PTDC/QEQ-MED/0262/2014), PT 2020/CENTRO 2020 (project no. CENTRO-01-0145-FEDER-000014/ MATIS) and CIMAGO Project 07/2018. Coimbra Chemistry Centre (CQC) is supported by FCT through project UIDB/00313/2020 and UIDP/QUI/00313/2020, co-funded by COMPETE2020-UE. CIBB, former CNC.IBILI, is funded by National Funds via FCT through the Strategic Projects UID/NEU/04539/2019, UIDB/04539/2020 and UIDP/04539/2020 and by COMPETE-FEDER (POCI-01-0145-FEDER-007440). We also acknowledge the UC-NMR facility for obtaining the NMR data (www.nmrccc.uc.pt).

REFERENCES

[1] S. Kwiatkowski, B. Knap, D. Przystupski, J. Saczko, E. Kędzierska, K. Knap-Czop, J. Kotlińska, O. Michel, K. Kotowski, J. Kulbacka, Photodynamic Therapy – Mechanisms, Photosensitizers and Combinations, Biomed. Pharmacother., 106 (2018) 1098-1107.https://doi.org/10.1016/j.biopha.2018.07.049.

[2] R. Falk-Mahapatra, S.O. Gollnick, Photodynamic Therapy and Immunity: An Update, Photochem. Photobiol,, early access (2020).https://doi.org/10.1111/php.13253

[3] D. Luo, K.A. Carter, D. Miranda, J.F. Lovell, Chemophototherapy: an Emerging Treatment Option for Solid Tumors, Adv. Sci., 4 (2017) 1-24.https://onlinelibrary.wiley.com/doi/abs/10.1002/advs.201600106

[4] H. Abrahamse, M.R. Hamblin, New photosensitizers for photodynamic therapy, Biochem. J. , 473 (2016) 347-364.https://doi.org/10.1042/BJ20150942

[5] D. Van Straten, V. Mashayekhi, H.S. De Bruijn, S. Oliveira, D.J. Robinson, Oncologic photodynamic therapy: basic principles, current clinical status and future directions, Cancers, 9 (2017) E19.https://www.ncbi.nlm.nih.gov/pubmed/28218708

[6] M.G. Dilkes, M.L. DeJode, A. Rowntree-Taylor, J.A. McGilligan, G.S. Kenyon, P. McKelvie, m-THPC photodynamic therapy for head and neck cancer., Lasers Med. Sci., 11 (1996) 23-29.https://link.springer.com/article/10.1007/BF02161289

[7] A.C. Kübler, J. de Carpentier, C. Hopper, A.G. Leonard, G. Putnam, Treatment of squamous cell carcinoma of the lip using Foscan-mediated Photodynamic Therapy., Int. J. Oral Surg., 30 (2001) 504−509.https://www.ncbi.nlm.nih.gov/pubmed/11829232

[8] M.P. Copper, I.B. Tan, H. Oppelaar, M.C. Ruevekamp, F.A. Stewart, meta-Tetra(hydroxyphenyl)chlorin photodynamic therapy in early-stage squamous cell carcinoma of the head and neck, Arch. Otolaryngol., Head Neck Surg., 129 (2003) 709-711.https://jamanetwork.com/journals/jamaotolaryngology/fullarticle/483893

[9] C. Hopper, A. Kübler, H. Lewis, I.B. Tan, G. Putnam, mTHPC-mediated photodynamic therapy for early oral squamous cell carcinoma, Int. J. Cancer, 111 (2004) 138-146.https://onlinelibrary.wiley.com/doi/10.1002/ijc.20209
[10] S.J. Isakoff, G.S. Rogers, S. Hill, P. McMullan, K.R. Habin, H. Park, D.W. Bartenstein, S.T. Chen, W.T. Barry, B. Overmoyer, An open label, phase II trial of continuous low-irradiance photo- dynamic therapy (CLIPT) using verteporfin for the treatment of cutaneous breast cancer metastases, J. Clin. Oncol., 35 (2017) TPS1121.https://ascopubs.org/doi/abs/10.1200/JCO.2017.35.15_suppl.TPS1121
[11] I.D. Fabian, A.W. Stacey, V. Papastefanou, L. Al Harby, A.K. Arora, M.S. Sagoo, V.M.L. Cohen, Primary photodynamic therapy with verteporfin for small pigmented posterior pole choroidal melanoma, Eye, 31 (2017) 519-528. https://doi.org/10.1038/eye.2017.22
[12] M.T. Huggett, M. Jermyn, A. Gillams, R. Illing, S. Mosse, M. Novelli, E. Kent, S.G. Bown, T. Hasan, B.W. Pogue, S.P. Pereira, Phase I/II study of verteporfin photodynamic therapy in locally advanced pancreatic cancer, Br. J. Canc., 110 (2014) 1698-1704.https://www.ncbi.nlm.nih.gov/pubmed/24569464
[13] J.W. Miller, U. Schmidt-Erfurth, M. Sickenberg, H. Laqua, I. Barbazetto, E.S. Gragoudas, L. Zografos, B. Piguet, C.J. Pournaras, G. Donati, A. Lane, R. Birngruber, H. van den Berg, H.A. Strong, U. Manjuris, T. Gray, M. Fsadni, N.M. Bressler, Photodynamic therapy with verteporfin for choroidal neo- vascularization caused by age-related macular degeneration: Results of a single treatment in a phase 1 and 2 study, Arch. Ophthalmol. , 117 (1999) 1161-1173.https://jamanetwork.com/journals/jamaophthalmology/fullarticle/412330
[14] W. Ji, J.-W. Yoo, E.K. Bae, J.H. Lee, C.-M. Choi, The effect of Radachlorin® PDT in advanced NSCLC: A pilot study, Photodiagn. Photodyn. Ther., 10 (2013) 120-126.https://www.sciencedirect.com/science/article/abs/pii/S1572100013000070
[15] E.V. Kochneva, E.V. Filonenko, E.G. Vakulovskaya, E.G. Scherbakova, O.V. Seliverstov, N.A. Markichev, A.V. Reshetnickov, 2010, 258− 267. , Photosensitizer Radachlorin® : Skin cancer PDT phase II clinical trials. , Photodiagn. Photodyn. Ther., 7 (2010) 258-267.https://www.ncbi.nlm.nih.gov/pubmed/21112549
[16] N.A.M.M. Pereira, M. Laranjo, J. Casalta-Lopes, A.C. Serra, M. Piñeiro, J. Pina, J.S. Seixas de Melo, M.O. Senge, M.F. Botelho, L. Martelo, H.D. Burrows, T.M.V.D. Pinho e Melo, Platinum(II) Ring-Fused Chlorins as Near-Infrared Emitting Oxygen Sensors and Photodynamic Agents, ACS Med. Chem. Lett., 8 (2017) 310-315.https://doi.org/10.1021/acsmedchemlett.6b00476
[17] N.A.M. Pereira, M. Laranjo, J. Pina, A.S.R. Oliveira, J.D. Ferreira, C. Sánchez-Sánchez, J. Casalta-Lopes, A.C. Gonçalves, A.B. Sarmento-Ribeiro, M. Pineiro, J.S. Seixas de Melo, M.F. Botelho, T.M.V.D. Pinho e Melo, Advances on Photodynamic Therapy of Melanoma through Novel Ring-Fused 5,15-Diphenylchlorins, Eur. J. Med. Chem., 146 (2018) 395-408.https://doi.org/10.1016/j.ejmech.2017.12.093
[18] N.A.M. Pereira, M. Laranjo, M. Pineiro, A.C. Serra, K. Santos, R. Teixo, A.M. Abrantes, A.C. Gonçalves, A.B. Sarmento Ribeiro, J. Casalta-Lopes, M.F. Botelho, T.M.V.D. Pinho e Melo, Novel 4,5,6,7-Tetrahydropyrazolo[1,5-a]Pyridine Fused Chlorins as Very Active Photodynamic Agents for Melanoma Cells, Eur. J. Med. Chem., 103 (2015) 374–380.https://doi.org/10.1016/j.ejmech.2015.08.059
[19] B.F.O. Nascimento, M. Laranjo, N.A.M. Pereira, J. Dias-Ferreira, M. Pineiro, M.F. Botelho, T.M.V.D. Pinho E Melo, Ring-Fused Diphenylchlorins as Potent Photosensitizers for Photodynamic Therapy Applications: In Vitro Tumor Cell Biology and in Vivo Chick Embryo Chorioallantoic Membrane Studies, ACS Omega, 4 (2019) 17244–17250.https://doi.org/10.1021/acsomega.9b01865.

[20] R.S. Kalash, V.K. Lakshmanan, C.-S. Cho, I.-K. Park, Theranostics. In Biomaterials Nanoarchitectonics, in: Elsevier (Ed.), 2016, pp. pp 197–215, https://doi.org/110.1016/B1978-1010-1323-37127-37128.00012-37121.
[21] M.L. Dean, J.R. Schmink, N.E. Leadbeater, C. Brückner, Microwave-Promoted Insertion of Group 10 Metals into Free Base Porphyrins and Chlorins: Scope and Limitations, Dalton Trans., 10 (2008) 1341-1345.https://pubs.rsc.org/en/content/articlelanding/2008/dt/b716181f - !divAbstract
[22] R. Teixo, M. Laranjo, A.M. Abrantes, G. Brites, A. Serra, R. Proença, M.F. Botelho, Retinoblastoma: Might Photodynamic Therapy Be an Option?, Cancer Metastasis Rev., 34 (2005) 563–573.https://doi.org/10.1007/s10555-014-9544-y.
[23] M. Obata, S. Hirohara, R. Tanaka, I. Kinoshita, K. Ohkubo, S. Fukuzumi, M. Tanihara, S. Yano, In Vitro Heavy-Atom Effect of Palladium(II) and Platinum(II) Complexes of Pyrrolidine-Fused Chlorin in Photodynamic Therapy., J. Med. Chem., 52 (2009) 2747–2753.https://doi.org/10.1021/jm8015427.
[24] J.-F. Chiou, Y.-H. Wang, M.-J. Jou, T.-Z. Liu, C.-Y. Shiau, Verteporfin-Photoinduced Apoptosis in HepG2 Cells Mediated by Reactive Oxygen and Nitrogen Species Intermediates, Free Radic. Res., 44 (2010) 155–170.https://doi.org/10.3109/10715760903380458.
[25] M. Conrad, J.P.F. Angeli, P. Vandenabeele, B.R. Stockwell, Regulated Necrosis: Disease Relevance and Therapeutic Opportunities. , Nat. Rev. Drug Discov. , 15 (2016) 348–366.https://doi.org/10.1038/nrd.2015.6.
[26] W. Armarego, D. Perrin, Purification of Laboratory Chemicals, 4th edition;, 1997.
[27] N.V. Chizhova, O.M. Kulikova, N.Z. Mamardashvili, Synthesis and Properties of Ms- and β-Substituted Pt(II) and Pt(IV) Tetraphenylporphyrinates., Russ. J. Gen. Chem., 83 (2013) 2108–2111.https://doi.org/10.1134/S107036321311025X.
[28] N.A.M. Pereira, A.C. Serra, T.M.V.D. Pinho e Melo, Novel Approach to Chlorins and Bacteriochlorins: [8π+2π] Cycloaddition of Diazafulvenium Methides with Porphyrins, Eur. J. Org. Chem., 2010 (2010) 6539–6543.https://doi.org/10.1002/ejoc.201001157.
[29] N.A.M. Pereira, S.M. Fonseca, A.C. Serra, T.M.V.D. Pinho e Melo, H.D. Burrows, [8π+2π] Cycloaddition of Meso-Tetra- and 5,15-Diarylporphyrins: Synthesis and Photophysical Characterization of Stable Chlorins and Bacteriochlorins, Eur. J. Org. Chem., 2011 (2011) 3970–3979.https://doi.org/10.1002/ejoc.201100465.
[30] M. Laranjo, A.C. Serra, M. Abrantes, M. Pineiro, A.C. Gonçalves, J. Casalta-Lopes, L. Carvalho, A.B. Sarmento-Ribeiro, A. Rocha-Gonsalves, F. Botelho, 2-Bromo-5-Hydroxyphenylporphyrins for Photodynamic Therapy: Photosensitization Efficiency, Subcellular Localization and in Vivo Studies, Photodiagnosis Photodyn. Ther., 10 (2013) 51-61.https://doi.org/10.1016/j.pdpdt.2012.05.003.

Platinum(II) Ring-Fused Chlorins as Efficient Theranostic Agents: Dyes for Tumor-Imaging and Photodynamic Therapy of Cancer

Highlights

- The discovery of Pt-chlorin-type theranostic agents is described
- Luminescent Pt(II)-chlorins with different degrees of hydrophilicity synthesized
- High phototoxicity against human melanoma, oesophageal and bladder carcinomas
- In vivo fluorescence imaging and PDT with the lead photosensitizer
- Biodistribution and pharmacokinetics using PS intrinsic bioluminescent properties

Declaration of interests

☒ The authors declare that they have no known competing financial interests or personal relationships that could have appeared to influence the work reported in this paper.

☐The authors declare the following financial interests/personal relationships which may be considered as potential competing interests:

Teresa M. V. D. Pinho e Melo
7 April 2020